Journal of Organometallic Chemistry 880 (2019) 253–260

Contents lists available at ScienceDirect

Journal of Organometallic Chemistry

journal homepage: www.elsevier.com/locate/jorganchem

Theoretical study on the intramolecular oxyamination involved in Rh(III)-catalyzed cyclization of unsaturated alkoxyamines

Siwei Bi*, Yueyue Wang, Yuan-Ye Jiang, Yuxia Liu

School of Chemistry and Chemical Engineering, Qufu Normal University, Qufu, 273165, PR China

ARTICLE INFO

Article history:
Received 15 October 2018
Received in revised form
6 November 2018
Accepted 13 November 2018
Available online 14 November 2018

Keywords:
Intramolecular oxyamination
Rh(III)-catalysis
Unsaturated alkoxyamine
Nitrene Rh(V) species
DFT calculation

ABSTRACT

The unexpected oxyamination reaction of *O*, ω-unsaturated alkoxyamines was found experimentally. The mechanistic issues were studied by DFT calculations. It is suggested that the reaction undergoes [3 + 2] cyclic addition, O–N bond cleavage, C–N reductive elimination, and the Rh–N unit protonation, generating the product and regenerating the active catalyst. The nitrene Rh(V) species containing a Rh–C bond rather than a Rh–O bond was suggested to be involved in the reaction mechanism. Why the substrate **A** with X = O but not X = C undergoes oxyamination reaction was rationalized based on the suggested reaction mechanism.

1. Introduction

Glorius [1], Cossy [2], and Rovis [3] have demonstrated that Rh(III) could be used as the catalyst to trigger allylic C(sp^3)–H activation/amination of unsaturated N-amides. The typical oxidative coupling reaction [4] eq 1 is shown in Scheme 1, which allows for intramolecular amination to generate the nitrogen-containing heterocyclic product **B**.[2] Based on the precedent researches, the Cossy group designed a reaction eq 2 [5] (Scheme 1) with the oxygen atom connecting to the nitrogen atom in substrate **A**, which differs from eq 1 with a carbon atom connecting to the nitrogen atom. The aim of designing eq 2 is expected to obtain **E**, a product formally similar to **B**, via allylic C–H activation, but they failed. Instead, they unexpectedly obtained product **C** via oxyamination of the carbon-carbon double bond. Also, product **D**, a product formally similar to **C**, was obtained experimentally. In summary, the reaction with X = C and O respectively gives completely distinct chemical reactivity. Eq 1 is an oxidative reaction with $Cu(OAc)_2$ acting as an oxidant.

This unexpected experiment of eq 2 is of significant importance because oxyamination of alkenes has drawn much attention in chemistry, biology and materials science [6]. Especially, the intramolecular oxyaminations with the substrates containing an N–O bond were rarely studied [7], and those previously reported reactions containing N–O bond were achieved with Cu(I), Fe(II) and light catalyses, which is distinct from the reaction eq 2 with Rh(III) catalysis. A literature search showed that reaction eq 2 is the first example of Rh(III)-catalyzed intramolecular oxyamination of unsaturated alkoxyamine that affords the product possessing a nitrogen-containing heterocycle.

In view of the unexpected discovery of reaction eq 2 and its applications in a variety of areas, further insights into these reactions are desired. Particularly, deep understanding of fundamental mechanistic scenarios is critical toward future design of synthetic transformations involving intramolecular oxyaminations. In this work, our computational study would focus on the mechanistic issues related to the intramolecular oxyamination of olefins, particularly to the experimentally proposed nitrene intermediate that needs to be further investigated.

2. Computational details

The geometry optimizations were conducted using the M06 functional [8], with LANL2DZ basis set [9] for rhodium and sulfur and 6-31G(d,p) basis set [10] for the other atoms. The M06 functional method has been demonstrated to be well applied in Rh-catalyzed organic syntheses [11]. To confirm whether each optimized stationary point is an energy minimum (zero imaginary

* Corresponding author.
E-mail address: siweibi@126.com (S. Bi).

https://doi.org/10.1016/j.jorganchem.2018.11.019
0022-328X/

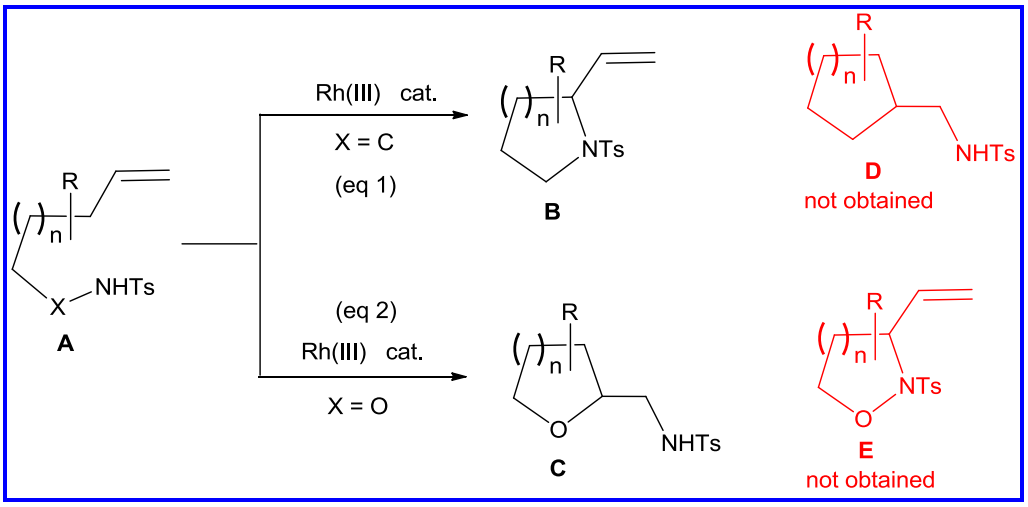

Scheme 1. Reactions involving allylic C–H activation (Eq 1) and oxyamination (Eq 2).

frequencies) or a transition state (only one imaginary frequency), as well as evaluate the zero-point vibrational energy and thermal corrections at 298 K, the vibrational frequencies were computed at the same level of theory as for the geometry optimizations [12]. The single-point energies and solvent effects were computed also with the M06 functional but the higher level SDD basis set [13] was used for rhodium and sulfur and the 6–311++G(d,p) basis set [14] for the other atoms, based on the gas-phase optimized structures. The solvation energies were evaluated by a self-consistent reaction field (SCRF) using the SMD implicit solvent model [15]. All density functional theory (DFT) calculations were performed by Gaussian 09 program [16].

3. Results and discussion

Experiments have demonstrated that reaction eq 2 has a broad substrate scope.2 The internal olefinic carbon and the α and β carbon relative to the C=C moiety could tolerate different substituents. Reaction eq 3 was experimentally demonstrated to give the highest yield, and thus we chose it as the title reaction in this study to probe the reaction mechanism and related issues.

We first illustrated the possible reaction pathways, and then gave the calculation results of the step corresponding to **K** + **I** → **II**, a common step for the different pathways proposed. Subsequently, we investigated the possible reaction pathways and suggested key intermediates. Finally, we explored the origin why the reaction is distinctive when X = C is replaced by X = O.

3.1. Reaction pathways to be examined

Based on their experimental results, the Cossy group presented some mechanistic hypotheses (path a, path b1 and path c in Scheme 3).5 The active catalyst $Cp^*Rh(OAc)_2$ (**K**) is firstly afforded by the reaction of the precatalyst $[Cp^*Rh(MeCN)_3](SbF_6)_2$ with $Cu(OAc)_2$. Then intermediate **II** is generated by H–N deprotonation. Path a is assigned to undergo a [3 + 2] cyclic addition to evolve into a five-membered rhodacyclic intermediate **III**, and subsequent N–O cleavage delivers intermediate **IV**. Finally, protonation of **IV** with acetate acid produces the final product **V** and regenerates the active catalyst **K**. Path b relates to the N–O oxidative addition, allowing for the generation of a nitrene intermediate **VI**. In path b1, coupling of the nitrene unit with the C=C double bond forms a three-membered azacycle (**VII**), which then evolves into **IV** by ring opening of the azacycle. Path c is proposed to be a direct transformation from **II** to **VII**.

Additionally, two plausible paths, path b2 and path d, were proposed in this work. In path b2, C=C insertion into the Rh–O bond gives intermediate **VIII** that then undergoes alkyl migration to the nitrene atom to afford **IV**. In path d, C=C insertion into the Rh–N bond delivers intermediate **IX** and then the O–N oxidative addition to the metal affords intermediate **X**. **X** undergoes N–C reductive elimination generating intermediate **VII**. The subsequent steps are the same as in path b1 (**VII** → **IV** → **V**).

The experimental authors conjectured that the reaction might undergo paths b1 or c. Thus, examining all the proposed pathways illustrated in Scheme 3 with the aid of DFT calculations is valuable, from which we anticipate to identify which one is the most reasonable.

3.2. N–H deprotonation of substrate *I*

As shown in Scheme 3, the step of N–H deprotonation of substrate **I** (**K** → **II**) is common for the subsequent paths. We first investigated the N–H deprotonation process with the aid of DFT calculations. Fig. 1 shows the DFT-computed Gibbs free changes for acetate-assisted N–H deprotonation in the title reaction eq 3. Consistent with the experimental suggestions [5], $Cp^*Rh(OAc)_2$ (**K**) was employed as the active catalyst, generated in situ from $[Cp^*Rh(MeCN)_3]SbF_6$ and $Cu(OAc)_2$. Coordination of the substrate **S** via nitrogen atom to Rh gives intermediate **1** that then undergoes a proton transfer giving intermediate **2**. The large entropy decrease from **K** + **S** to **1** arises from the calculation in gas phase. Considering the transformations in Fig. 1 are not rate-determining, we did not make entropy corrections. The proton transfer from N to O is kinetically facile with a puny barrier of 0.4 kcal/mol **2** being slightly less stable than **TS1** in Gibbs free energy is due to the consideration of thermal corrections. Release of the resulting acetate acid delivers intermediate **3** with the C=C bond weakly coordinated to the metal center. Replacement of the C=C coordination with acetate oxygen gives **3a**. The Rh–N bond length decreases from **1** to **3** with the proton moving from N to O, indicating the proton transfer enhances the Rh–N bond. From this energy change diagram one can see the deprotonation process is both kinetically and thermodynamically feasible.

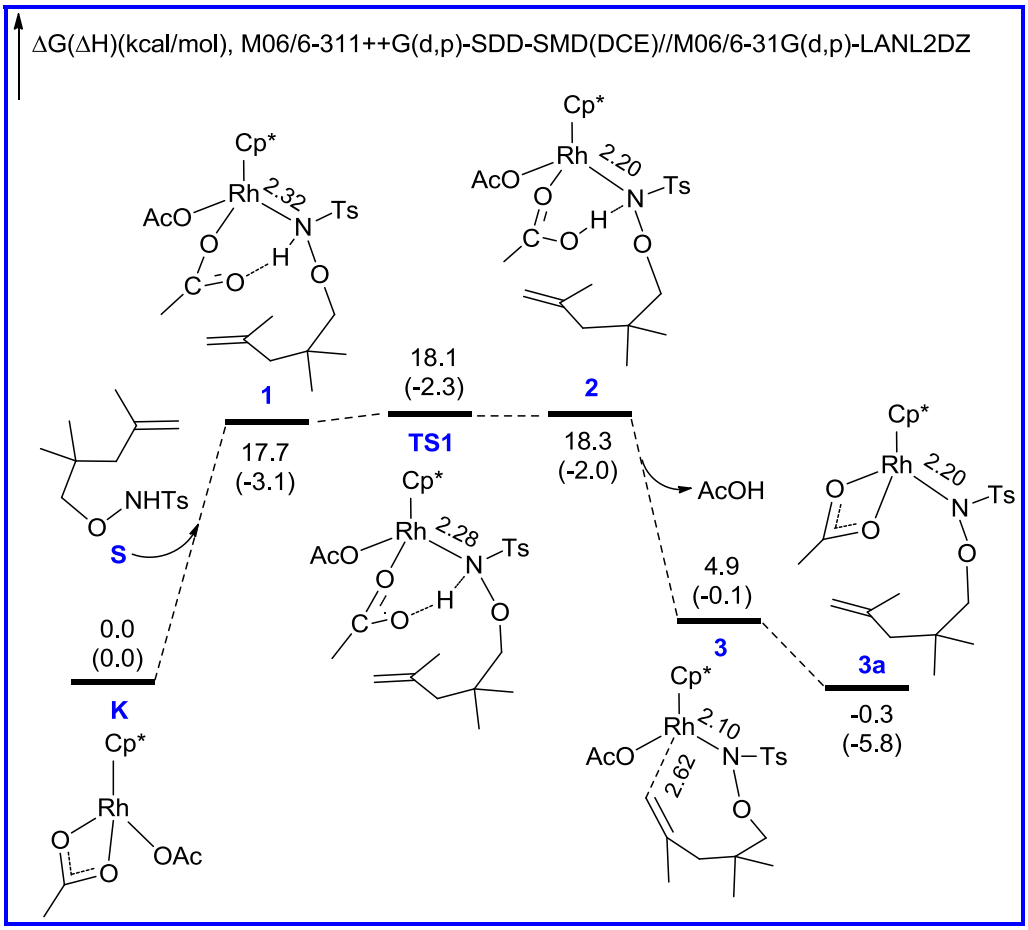

Fig. 1. DFT-computed Gibbs free changes of the N-H deprotonation process. The bond lengths are given in degree (Å). The relative Gibbs free energies and the enthalpies (in parentheses) are given in kcal/mol.

3.3. Mechanism of path a

For path a in Scheme 3, the [3 + 2] cyclic addition (**II**→**III**) followed by ring fragmentation (**III**→**IV**) is proposed. The energy profile calculated for path a based on eq 3 in Scheme 2 was presented in Fig. 2. The [3 + 2] cyclic addition allows for formation of C–O and Rh–C bond (**3** → **4**), which is kinetically achievable but thermodynamically unfavorable with the energy span from **3** to **4** being 13.4 kcal/mol. Slight elongation of the N–O bond from **3** (1.41 Å) to **4** (1.48 Å) indicates the N–O bond is sort of activated. **4** has clearly a zwitterionic structure. The next N–O bond cleavage (**4** → **5**) has a small activation barrier of 4.7 kcal/mol and both **4** and **5** have similar stability. It is noteworthy that the N–O cleavage enables the metal center to be oxidized to afford a Rh(V) nitrene intermediate (**5**), which was not mentioned in path a of Scheme 3. After that, the C–N reductive elimination occurs to give the significantly stable Rh(III) intermediate **6**. Clearly the C–N bond formation is the thermodynamic driving force for the process from **3** to **6**.

The following steps are related to the protonation of the Rh-bonded nitrogen atom. Addition of a HOAc molecule into **6** evolves into intermediate **7**, where the oxygen coordination of Ts group is replaced by the oxygen of HOAc. The relatively great Gibbs energy increase from **6** to **7** arises mainly from the entropy decrease due to the two-to-one transformation. Then, the proton transfer form nitrogen to oxygen takes place via a puny barrier to produce the product-coordinated intermediate **8**. Finally, release of the product from the metal center delivers the product **P** and regenerates the active catalyst **K**, completing the catalytic cycle.

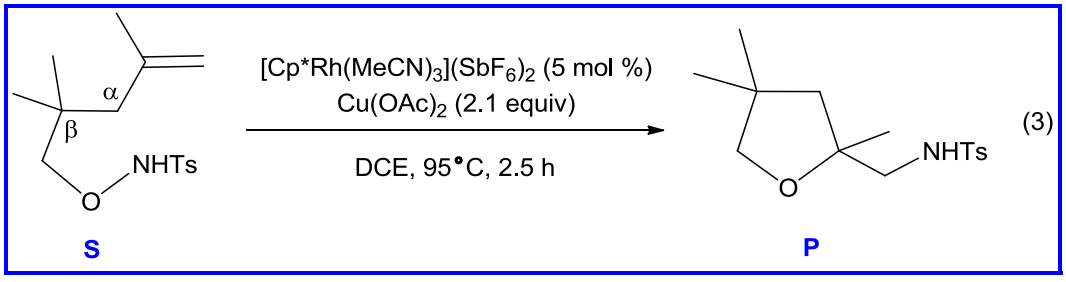

Scheme 2. Title reaction studied in this work.

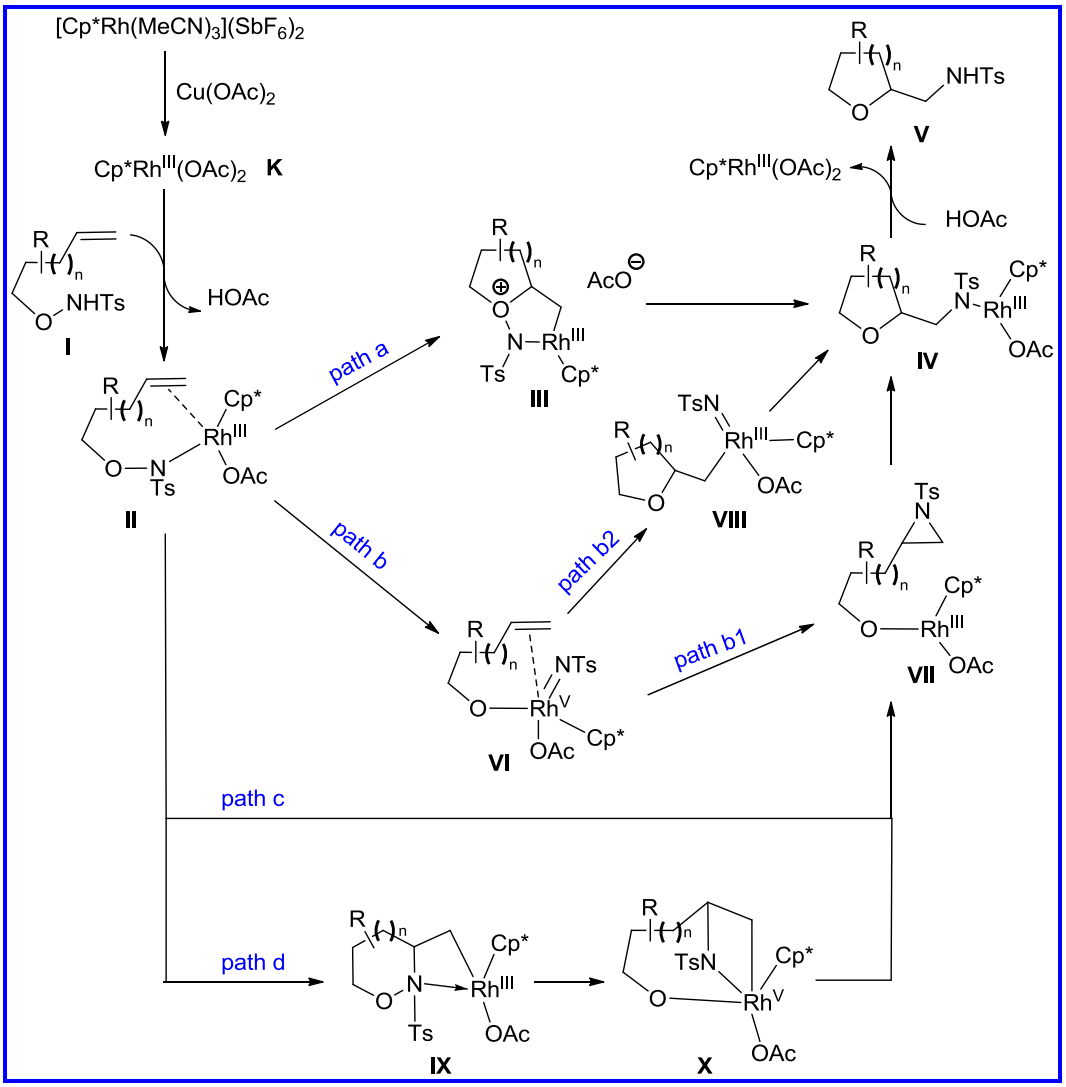

Scheme 3. Plausible reaction mechanisms.

In summary, path a involves cyclic C–O coupling, O–N cleavage, C–N reductive elimination, and protonation of Rh-bound nitrogen to produce the product. The C–N reductive elimination step is rate-determining with an overall barrier of 26.9 kcal/mol, and this step is the major thermodynamic driving force to render the reaction forward. Notably, a Rh(V) nitrene intermediate (**5**) of the pathway is disclosed in this study.

3.4. Mechanism of path b

As proposed in Scheme 3, path b involves N–O oxidative addition to afford the Rh(V) intermediate **VI** from which paths b1 and b2 were proposed. We first examine the feasibility of **VI**. As shown in Fig. 3, the N–O oxidative addition step is calculated to have a high lying barrier of 50.0 kcal/mol and the energy span from **3** to **9** (corresponding to **VI**) is 35.9 kcal/mol. Clearly, this oxidative addition step is unachievable, due to the thermodynamic instability of **9**. In summary, the Rh(V) nitrene intermediate **9** is found to be significantly unstable, and thus we suggested that the Rh(V) nitrene intermediate **9** (corresponding to **VI**) is not involved in the reaction mechanism. Path b (including paths b1 and b2) can be precluded.

It is of great value to understand why the Rh(V) nitrene intermediate **5** is significantly more stable than the Rh(V) nitrene intermediate **9**. The electronic energy difference between **5** and **9** is calculated to be 20.3 kcal/mol, which can be attributed to the following factors: a) the breaking Rh–O bond is less stable than the forming Rh–C bond; b) the breaking C=C π bond is less stable than the forming O–C bond. A similar relative stability of **5-H** vs **9-H** was also found, where the metallic fragment is replaced by hydrogen (Scheme 4). The energy difference between **9-H** and **5-H** is −18.1 kcal/mol, similar to the one between **9** and **5** (−20.3 kcal/mol). It is revealed form above analysis that direct N–O oxidative addition from intermediate **3** to generate a pendent alkoxyl group unachievable both thermodynamically and kinetically. Instead, first [3 + 2] cyclic addition followed by O–N bond cleavage, which leads to the Rh–C bond formation and organic cyclization, enables the Rh(V) nitrene intermediate relatively more stable and thus achievable under the reaction conditions.

3.5. Mechanism of path c

As shown in path c of Scheme 3, a direct transformation from **II** to **VII** was experimentally hypothesized. For examining the above mechanistic hypothesis, we made best effort to locate the transition

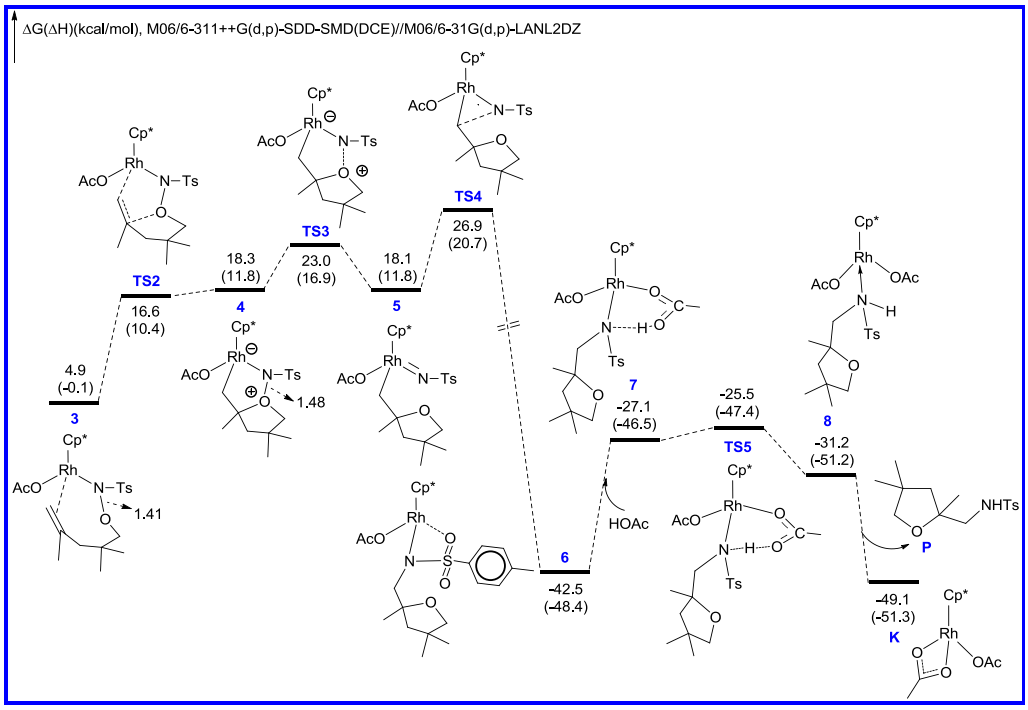

Fig. 2. DFT-computed Gibbs free changes of path a. The bond lengths are given in degree (Å). The relative Gibbs free energies and the enthalpies (in parentheses) are given in kcal/mol.

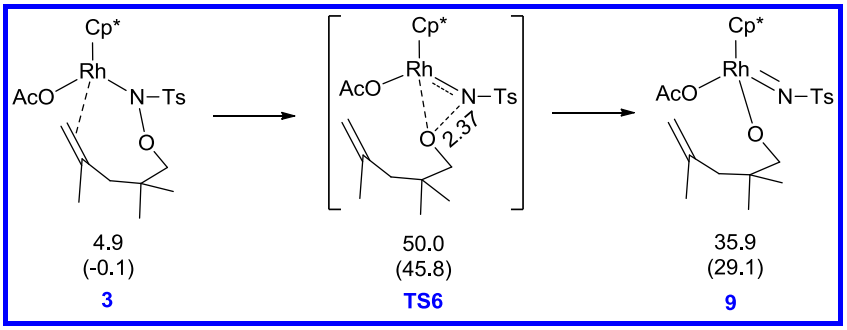

Fig. 3. DFT-computed Gibbs free changes of path b. The bond lengths are given in degree (Å). The relative Gibbs free energies and the enthalpies (in parentheses) are given in kcal/mol.

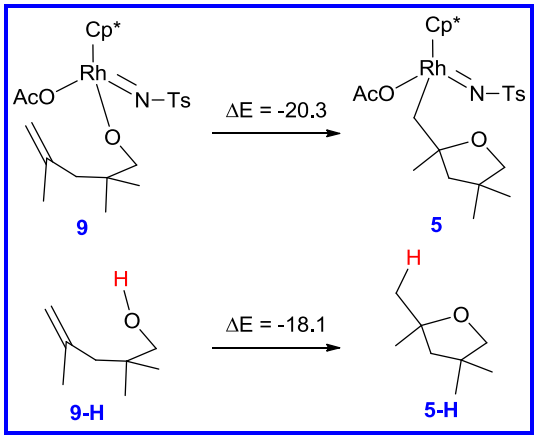

Scheme 4. Energy difference of 5 and 9 *vs* 5-H and 9-H (kcal/mol).

state that directly connects **3** and **11** (corresponding to **II** and **VII**), but we failed to locate such a transition state. Instead, we located the transition state **TS7** that connects **10** and **11** (Fig. 4). **10** is structurally different from **3**, with oxygen bound to the metal. The step **11** to **6** via **TS8** undergoes a N–C and Rh–O σ bond metathesis to afford **6**. This path is infeasible with a barrier as high as 58.5 kcal/mol and thus can be excluded.

If the transition state **TS12** that directly connects **3** and **11** as illustrated in Scheme 5 were existent, there would be concurrently three bonds a, b and c being broken and three bonds d, e and f being formed. Too many bonds (see the structure of **TS12**) are involved in bond breaking and bond forming in one elementary step, and we think such a scenario is kinetically difficult. Therefore as demonstrated by our calculations that the transition state **TS12** cannot be located. Based on our analysis and computation, the proposal for one-step from **II** to **VII** (path c) can be ruled out.

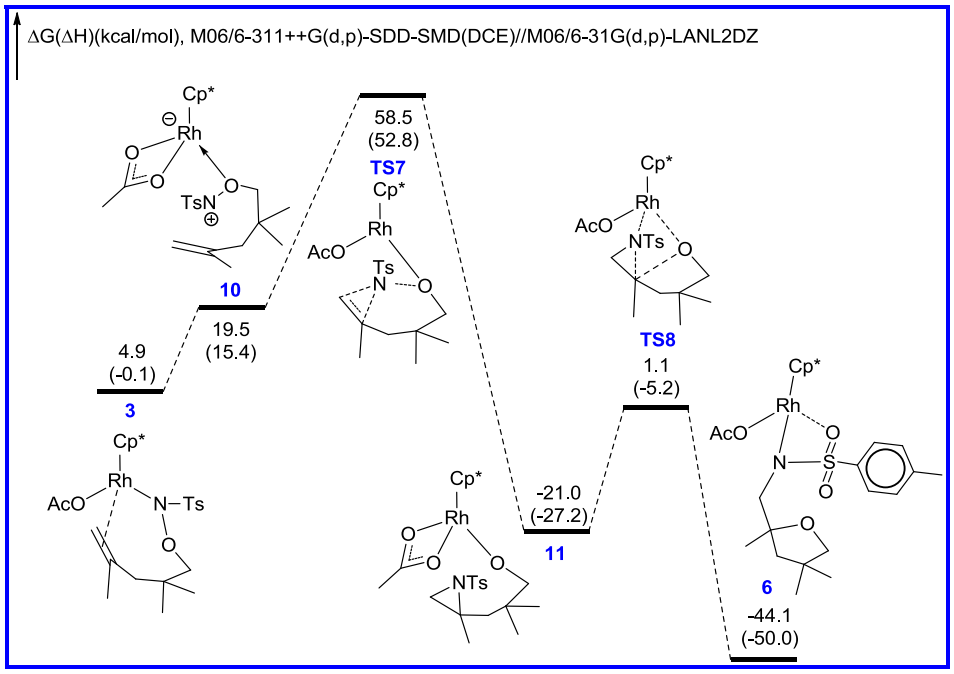

Fig. 4. DFT-computed Gibbs free changes of path c. The bond lengths are given in degree (Å). The relative Gibbs free energies and the enthalpies (in parentheses) are given in kcal/mol.

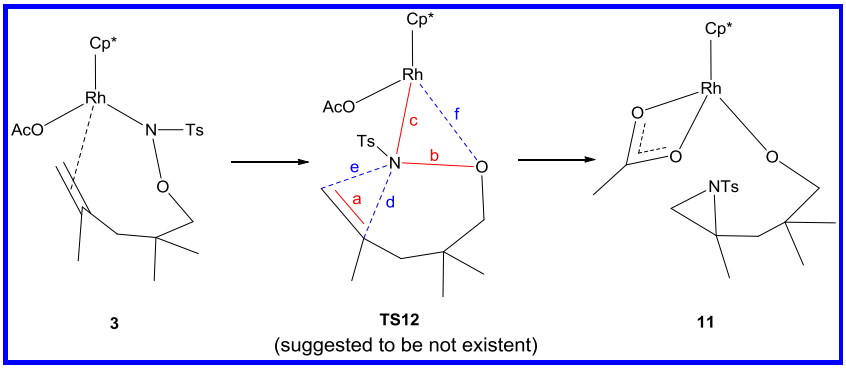

Scheme 5. Illustration of transition state **TS12** directly connecting **3** and **11**.

3.6. Mechanism of path d

Corresponding to the proposed path d as shown in Scheme 3, we performed the calculations related to C═C insertion into the Rh–N bond, based on the title reaction eq 3 (Fig. 5). This path was proposed as follows. C═C insertion into Rh–N gives **12**, and then N–O oxidative addition to Rh affords **13**. Subsequently, **13** undergoes C–N reductive elimination to afford a three-membered azacarbocycle **14** from which **11** can be delivered via coordination isomerism. Calculations indicated that, although the C═C insertion seems kinetically achievable, the subsequent oxidative addition from **12** to **13** is unachievable due to the high activation barrier. Considering inviability of the step **12** → **13**, further calculations on the following steps **13** → **14**→**11** were not performed.

On the basis of the above calculation results and analysis, the mechanistic information can be summarized as follows. (1) Path a is suggested to be the most reasonable mechanism in terms of the energetics calculated. (2) Path b is infeasible due to the high instability of the oxidative addition intermediate, the Rh(V) nitrene species **9**. (3) Paths c and d are also infeasible due to the unachievable kinetics for formation of intermediate **11** (corresponding to **VII** in Scheme 3) although it is quite stable thermodynamically.

3.7. Comments on the reaction mechanism

The experimental authors had given a hypothesis on mechanistic scenario of the reaction. They supposed an aziridine intermediate that was involved in the reaction, which could be generated from **II** by N–O oxidative addition (path b1) or direct transformation (path c) (Scheme 3). However, our computational results are not supportive of the hypothesis. The reason is that the two paths they proposed are difficult to proceed; path b1 is not achievable due to high instability of the involved nitrene Rh(V) intermediate; path c could not be reached due to the fact that there are too many breaking and forming bonds concurrently in one elementary step (a direct transformation).

Instead, based on our computational results, we proposed path a to be the suitable mechanism for the reaction studied with this path having an obviously favored low-lying energy profile. And,

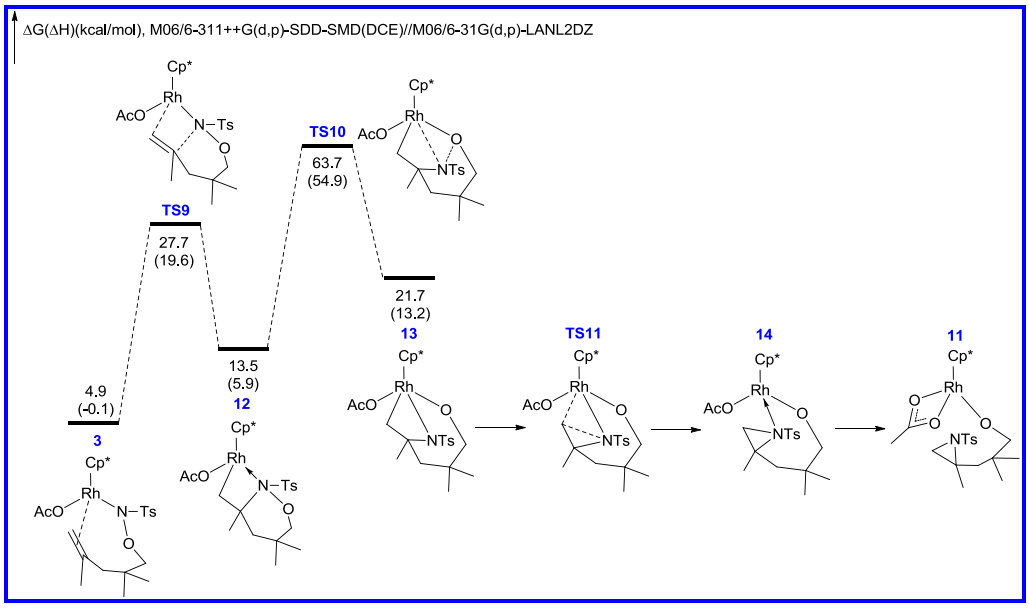

Fig. 5. DFT-computed Gibbs free changes of path d. The bond lengths are given in degree (Å). The relative Gibbs free energies and the enthalpies (in parentheses) are given in kcal/mol.

more remarkable, a nitrene Rh(V) intermediate was also disclosed in this study. The advantage of path a lies in the more stable Rh–C bond generation in the Rh(V) species, together with the favorable organic cyclization linked to the Rh–C carbon atom. The disadvantage of direct N–O oxidative addition to Rh(III) from **II** arises from the formed nitrene Rh(V) intermediate containing an unstable Rh–O bond.

Another issue is why the reaction shown in Scheme 1 switches from undergoing allylic C–H activation to oxyamination when the X in substrate **A** is changed from carbon to oxygen. This question can be rationalized from the preferred mechanism we suggested in this study (path a, Fig. 2). The [3 + 2] cyclic addition was suggested to allow for the C–O bond formation; subsequent N–O bond cleavage generates the nitrene Rh(V) intermediate that continuously undergoes C–N reductive elimination to recover the oxidation number of Rh to III from V. The reductive elimination step was suggested to be rate-determining. The electronic behaviors of the [3 + 2] cyclic addition process with X = O and X = C are shown in Scheme 6. The π electron pair is used to move forward to Rh to form a Rh–C σ bond. In **4** with X = O, the lone pair of oxygen moves toward the olefinic carbon to form a C–O σ bond, but in **4′** with X = C, the C–C σ bond cannot be formed because the carbon atom bears no electron pair. In fact, geometry optimization demonstrated that **4′** is not existent. Therefore, the species with X = O can undergo a [3 + 2] cyclic addition, while the one with X = C cannot.

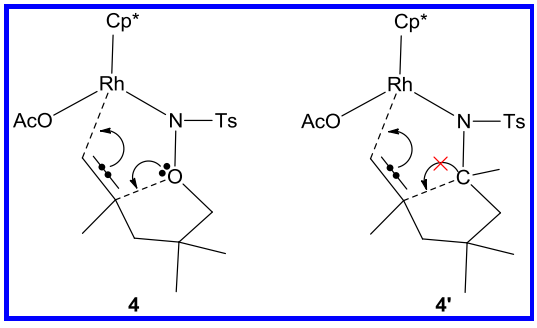

Scheme 6. Electronic behaviors of [3 + 2] cyclic addition with X = O and C.

4. Conclusions

The oxyamination reaction of *O*, ω-unsaturated alkoxyamines producing an O-containing heterocyclic product was unexpectedly found experimentally, with the initial goal attempting to obtain a N-containing heterocyclic product via allylic C–H activation. The mechanism of the reaction was characterized with the DFT calculations. The findings obtained through the theoretical and computational investigation are summarized as follows.

1) Among all the possible reaction paths proposed in Scheme 3, path a was suggested to be the most suitable for the reaction studied in this work. A [3 + 2] cyclic addition was proposed to generate a Rh–C and a C–O bond; then the O–N bond cleavage followed by C–N reductive elimination occurs, where the C–N reductive elimination is suggested to be rate-determining and a major thermodynamic driving force for the reaction; finally, protonation of the Rh–N unit delivers the product and regenerates the active catalyst.
2) A nitrene Rh(V) species was suggested to be involved in the reaction pathway, but it contains a stable Rh–C bond generated by [3 + 2] cyclic addition, O–N bond cleavage and C–N reductive elimination, rather than a Rh–O bond by N–O oxidative addition.
3) The lone pair of the oxygen atom is found to assist the [3 + 2] addition allowing for the C–N bond formation, whereas this addition cannot be achieved when oxygen is replaced by carbon atom due to the carbon lack of lone pair of electrons.

Notes

The authors declare no competing financial interests.

Acknowledgements

This work was jointly supported by the National Natural Science Foundation of China (Nos. 21473100, 21873055, 21702119).

Appendix A. Supplementary data

Supplementary data to this article can be found online at https://doi.org/10.1016/j.jorganchem.2018.11.019.

References

[1] S. Rakshit, F.W. Patureau, F. Glorius, J. Am. Chem. Soc. 132 (2010) 9585–9587.
[2] T. Cochet, V. Bellosta, D. Roche, J.-Y. Ortholand, A. Greiner, J. Cossy, Chem. Commun. 48 (2012) 10745–10747.
[3] A. Archambeau, T. Rovis, Angew. Chem. Int. Ed. 54 (2015) 13337–13340.
[4] I. Funes-Ardoiz, F. Maseras, ACS Catal. 8 (2018) 1161–1172.
[5] J. Escudero, V. Bellosta, J. Cossy, Angew. Chem. Int. Ed. 57 (2018) 574–578.
[6] (a) F. Cardona, A. Goti, Nat. Chem. 1 (2009) 269–275;
(b) T.J. Donohoe, C.K.A. Callens, A. Flores, A.R. Lacy, A.H. Rathi, Chem. Eur. J. 17 (2011) 58–76.
[7] (a) G.S. Liu, Y.Q. Zhang, Y.A. Yuan, H. Xu, J. Am. Chem. Soc. 135 (2013) 3343–3346;
(b) Y.Q. Zhang, Y.A. Yuan, G.S. Liu, H. Xu, Org. Lett. 15 (2013) 3910–3913;
(c) X. Ren, Q. Guo, J. Chen, H. Xie, Q. Xu, Z. Lu, Chem. Eur. J. 22 (2016) 18695–18699.
[8] (a) S.R. Neufeldt, G. Jimenez-Osés, J.R. Huckins, O.R. Thiel, K.N. Houk, J. Am. Chem. Soc. 137 (2015) 9843–9854;
(b) Y. Zhao, D.G. Truhlar, Theor. Chem. Acc. 120 (2008) 215–241;
(c) Y. Zhao, D.G. Truhlar, Acc. Chem. Res. 41 (2008) 157–167.
[9] (a) P.J. Hay, W.R. Wadt, J. Chem. Phys. 82 (1985) 270–283;
(b) P.J. Hay, W.R. Wadt, J. Chem. Phys. 82 (1985) 299–310.
[10] J. Andzelm, S. Huzinaga, Gaussian Basis Sets for Molecular Calculations, Elsevier Science, New York, 1984.
[11] (a) W. Wu, Y. Liu, S. Bi, Org. Biomol. Chem. 13 (2015) 8251–8260;
(b) W. Guo, T. Zhou, Y. Xia, Organometallics 34 (2015) 3012–3020.
[12] Z.-Y. Xu, S.-Q. Zhang, J.-R. Liu, P.-P. Chen, X. Li, H.-Z. Yu, X. Hong, Y. Fu, Organometallics 37 (2018) 592–602.
[13] (a) M. Dolg, U. Wedig, H. Stoll, H. Preuss, J. Chem. Phys. 86 (1987) 866–872;
(b) P. Schwerdtfeger, M. Dolg, W.H.E. Schwarz, G.A. Bowmaker, P.D.W. Boyd, J. Chem. Phys. 91 (1989) 1762–1774.
[14] C. Deng, W.H. Lam, Z.Y. Lin, Organometallics 36 (2017) 650–656.
[15] A.V. Marenich, C.J. Cramer, D.G. Truhlar, J. Phys. Chem. B 113 (2009) 6378–6396.
[16] M.J. Frisch, G.W. Trucks, H.B. Schlegel, G.E. Scuseria, M.A. Robb, J.R. Cheeseman, G. Scalmani, V. Barone, B. Mennucci, G.A. Petersson, H. Nakatsuji, M. Caricato, X. Li, H.P. Hratchian, A.F. Izmaylov, J. Bloino, G. Zheng, J.L. Sonnenberg, M. Hada, M. Ehara, K. Toyota, R. Fukuda, J. Hasegawa, M. Ishida, T. Nakajima, Y. Honda, O. Kitao, H. Nakai, T. Vreven, J.A. Montgomery, J.E. Peralta Jr., F. Ogliaro, M. Bearpark, J.J. Heyd, E. Brothers, K.N. Kudin, V.N. Staroverov, R. Kobayashi, J. Normand, K. Raghavachari, A. Rendell, J.C. Burant, S.S. Iyengar, J. Tomasi, M. Cossi, N. Rega, J.M. Millam, M. Klene, J.E. Knox, J.B. Cross, V. Bakken, C. Adamo, J. Jaramillo, R. Gomperts, R.E. Stratmann, O. Yazyev, A.J. Austin, R. Cammi, C. Pomelli, J.W. Ochterski, R.L. Martin, K. Morokuma, V.G. Zakrzewski, G.A. Voth, P. Salvador, J.J. Dannenberg, S. Dapprich, A.D. Daniels, Farkas, J.B. Foresman, J.V. Ortiz, J. Cioslowski, D.J. Fox, Gaussian 09, Revision D.01, Gaussian, Inc., Wallingford, CT, 2009.